# Self-Assembly and Nonlinear Dynamics of Dimeric Colloidal Rotors in Cholesterics

J. S. Lintuvuori,[1] K. Stratford,[2] M. E. Cates,[1] and D. Marenduzzo[1]

[1]SUPA, School of Physics and Astronomy, University of Edinburgh, Mayfield Road, Edinburgh, EH9 3JZ, United Kingdom
[2]EPCC, School of Physics and Astronomy, University of Edinburgh, Mayfield Road, Edinburgh, EH9 3JZ, United Kingdom

(Received 1 July 2011; published 23 December 2011)

We study by simulation the physics of two colloidal particles in a cholesteric liquid crystal with tangential order parameter alignment at the particle surface. The effective force between the pair is attractive at short range and favors assembly of colloid dimers at specific orientations relative to the local director field. When pulled through the fluid by a constant force along the helical axis, we find that such a dimer rotates, either continuously or stepwise with phase-slip events. These cases are separated by a sharp dynamical transition and lead, respectively, to a constant or an ever-increasing phase lag between the dimer orientation and the local nematic director.

DOI: 10.1103/PhysRevLett.107.267802 PACS numbers: 61.30.Jf, 47.57.J−, 83.80.Xz

Self-assembly is one of the key aims of present-day nanotechnology. The idea underpinning this concept is that, through a careful control of the interactions in a suspension of particles, it is possible to drive the spontaneous formation of an ordered target structure or pattern, starting from a disordered initial condition. The process is spontaneous as it often entails the minimization, whether global or local, of the free energy of the system. An outstanding specific challenge in modern self-assembly is to build a structure with a target dynamic feature, such as a synthetic microscopic rotor, walker, or swimmer [1].

Colloidal dispersions in liquid crystals offer a useful system for the development of self-assembly strategies at the microscale. Even in nematics, the simplest liquid crystalline phase, elastic distortions, and topological defects mediate a variety of interactions resulting in the formation of wires, colloidal crystals, cellular solids, and clusters entangled by disclinations [2–4]. This variety of self-assembled structures is possible because one can tune the liquid crystal mediated interactions by changing, e.g., the strength and nature of the liquid crystal ordering at the colloidal surface. These alter the local symmetry of the director field near the particle and hence qualitatively change the effective interparticle forces.

Here we show that a powerful way to extend the potential for self-assembly of colloids in liquid crystals is to consider cholesterics, or chiral nematics. In cholesterics the direction of the molecular order in the ground state spontaneously twists. The spatial modulation of the twist is in the micron range, therefore of the order of typical colloidal sizes. We have previously shown [5] that by varying the ratio between these two fundamental length scales, it is possible to change continuously the topology of the defects, or disclination lines, surrounding a single particle—morphological changes with no direct counterpart in nematics. Very recently, Mackay and Denniston [6] took a step further and studied the interparticle elastic force felt in a cholesteric by two colloidal spheres with tangential anchoring of the director field at their surface. As in the nematic case [7], there is a complex interplay between repulsive and attractive directions which leads to the formation of a dimer or longer chains. Here we focus on the simplest case of a dimer, but progress beyond the purely static investigation of [6] to show that such a dimer exhibits unexpected and intriguing dynamical properties. When subjected to an external force (for instance gravity) along the cholesteric helix, the dimer rotates about this axis in a screwlike fashion. Depending on the magnitude of the force, the dimer either rotates continuously or exhibits phase slippage, alternating periods of smooth rotation with static spells in which it translates without rotation. This dynamical transition shows similar near-critical behavior to the depinning of driven vortices and of charged density waves in superconductors, both of which may be studied with the Frenkel-Kontorova model for transport in a periodic potential [8]. Another analogue is provided by the synchronization of coupled oscillators described by the Kuramoto model [9]. Within our liquid crystal context, the phase slippage regime requires a specific free energy landscape which we discuss. This provides potential for the design of self-assembled systems with tunable dynamic properties.

The system we study consists of two spherical colloidal particles of radius $R$ moving in a cholesteric liquid crystal. To describe the thermodynamics of the chiral host, we employ a Landau–de Gennes free energy $\mathcal{F}$, whose density $f$ may be expressed in terms of a traceless and symmetric tensor order parameter $\mathbf{Q}$ [10] and is detailed in [11]. Tangential anchoring is modeled by a surface free energy, $f_s = \frac{1}{2}W(Q_{\alpha\beta} - Q^0_{\alpha\beta})^2$, where $W$ is the strength of anchoring and $Q^0_{\alpha\beta}$ is the preferred order parameter in the tangent plane to the local spherical surface [12].

We employ a 3D hybrid lattice Boltzmann (LB) algorithm [13] to solve the Beris-Edwards equations for $\mathbf{Q}$ [10]

$$D_t\mathbf{Q} = \Gamma\left[\frac{-\delta\mathcal{F}}{\delta\mathbf{Q}} + \frac{1}{3}\,\mathrm{tr}\left(\frac{\delta\mathcal{F}}{\delta\mathbf{Q}}\right)\mathbf{I}\right]. \quad (1)$$

 

Here, $\Gamma$ is a collective rotational diffusion constant and $D_t$ is the material derivative for rodlike molecules [10]. The term in brackets is known as the molecular field, which in the absence of flow drives the system towards a free energy minimum. The boundary conditions for the order parameter on the colloidal surfaces are given by [4]

$$\nu_\gamma \frac{\partial f}{\partial \partial_\gamma Q_{\alpha\beta}} + \frac{\partial f_s}{\partial Q_{\alpha\beta}} = 0, \tag{2}$$

where $\nu_\gamma$ is the local normal to the colloid surface.

The velocity field obeys the continuity and Navier-Stokes equation, with a stress tensor generalized to describe liquid crystal hydrodynamics [10]. Within our hybrid scheme, we solve the Navier-Stokes equation via LB, and Eq. (1) via finite difference [5]. Colloids are represented by the standard method of bounceback on links, which leads to a no-slip boundary condition for the velocity field (see [5,14] for details). Order parameter variations create an additional elastic force acting on the particle which is computed by integrating the stress tensor over the particle surface [4,5].

The dynamics is primarily controlled by the Ericksen number, $\mathrm{Er} = \gamma_1 v R/K$, where the rotational viscosity $\gamma_1 = 2q^2/\Gamma$, $v$ is a velocity characteristic of the flow, and $q$ is the degree of ordering in the system. In the uniaxial case with director $\hat{\mathbf{n}}$, $Q_{\alpha\beta} = q(\hat{n}_\alpha \hat{n}_\beta - \delta_{\alpha\beta}/3)$.

In what follows, we quote our results in simulation units [11,13]. To convert them into physical ones, we can specify an elastic constant of 28.6 pN, and a rotational viscosity of 1 P. (These values hold for typical materials, and a colloidal diameter of 1 $\mu$m.) In this way, the simulation units for force, time, and velocity can be mapped onto 440 pN, 1 $\mu$s, and 0.07 $\mu$m/s, respectively.

We first consider the interparticle elastic potential. Two particles are placed center-center separation vector $\mathbf{d}$ apart. Both particles are held fixed for the duration of a simulation in which the free energy is minimized. By repeating simulations for different $\mathbf{d}$, we map out the effective two-body potential as a function of the reduced separation $(d - 2R)/p$ in the three coordinate directions, and as a function of angle in the $x$-$y$ plane [Fig. 1(a)]. The potential is markedly anisotropic. While the potential in $z$ shows strong repulsion at large separations, there is an attraction in the $x$-$y$ plane. The most favorable configuration at small separations is along the director field [$x$ direction in Fig. 1(a)]. Here we estimate a maximum attractive force of 20 pN. Before this deep minimum is reached the dimer needs to overcome a repulsion [peak at $(d - 2R)/p \approx 0.2$], which is the largest when the disclinations at the opposing particle surfaces join up. In this bound state, the colloids share two disclination lines which act as a glue between them [right, Fig. 1(b)]. For separation vectors perpendicular to $\hat{\mathbf{n}}$ we find a stable minimum and no repulsive barrier [$y$ direction in Fig. 1(a)]. These results are far from the nematic limit studied experimentally in [7] and theoretically in [15], as well as from results obtained in a twisted nematic cell [16]. Most notably, the in-plane potential perpendicular to $\hat{\mathbf{n}}$ (here $y$) was always repulsive in the nematic [15]. The preferred configuration (here, along $\hat{\mathbf{n}}$) is at an angle of about 30° in the nematic [7,15].

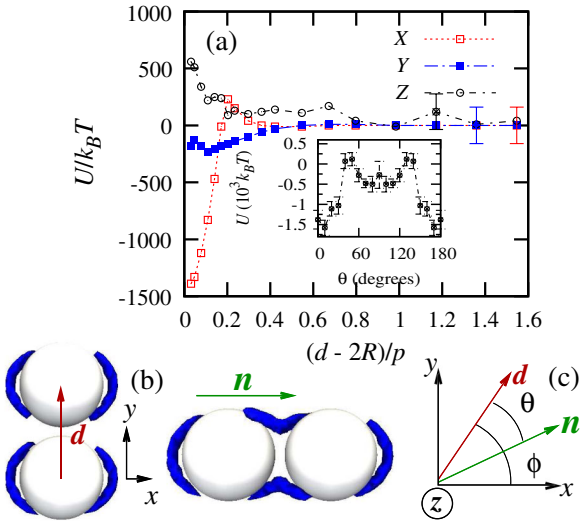


FIG. 1 (color online). (a) Interparticle elastic potential as a function of reduced separation $(d - 2R)/p$, along the helical axis ($z$) and in the $x$ and $y$ directions. The inset shows the angular dependence in the $x$-$y$ plane at $(d - 2R)/p \approx 0.05$. Units are in $k_BT \approx 4$ pN nm. (b) Snapshots of the dimer showing the disclination lines at $(d - 2R)/p \approx 0.05$ when $\mathbf{d}$ is along $y$ and along $x$. The Cartesian axes, the separation $\mathbf{d}$, and the far-field nematic director $\hat{\mathbf{n}}$ are shown. (c) Definition of the angles $\theta$ and $\phi$ used in the text. For error analysis see Supplemental Material [11].

These results confirm and extend those of [6] on the energetics of dimer formation in cholesterics. Our key focus in the present work is dynamics. We place two particles initially near the weaker minimum of the potential in the direction perpendicular to $\hat{\mathbf{n}}$ [left, Fig. 1(b)]. This is the first relatively deep local minimum two particles approaching from far away would encounter. It is therefore a natural self-assembled configuration for the dimer. We then pull each along the helical axis with force $f$.

At all force levels studied here, the moving dimer rotates about its center of mass while $\mathbf{d}$ remains perpendicular to the helical axis [inset, Fig. 2(e)]. The behavior at low force ($f \leq 0.025$) is illustrated in Figs. 2(a)–2(d). We quantify the rotation by measuring the angle $\phi$ between $\mathbf{d}$ and the $x$ axis and the angle $\theta$ between $\mathbf{d}$ and $\hat{\mathbf{n}}(z)$ [Fig. 1(c)], as a function of time. After an initial transient, a smooth rotation is observed [Fig. 2(e); open symbols], but with separation $\mathbf{d}$ that lags behind $\hat{\mathbf{n}}(z)$ by a constant phase angle $\theta(t)$ [Fig. 2(f), open symbols] [17]. We attribute this constant lag to a balance between the viscous drag opposing the rotation of the pair in the $x$-$y$ plane, and the force arising from the angular variation in the rotating interparticle potential.

At higher force ($f \geq 0.0275$), the behavior is manifestly different. The angle between $\mathbf{d}$ and $x$, shown in Fig. 2(e)

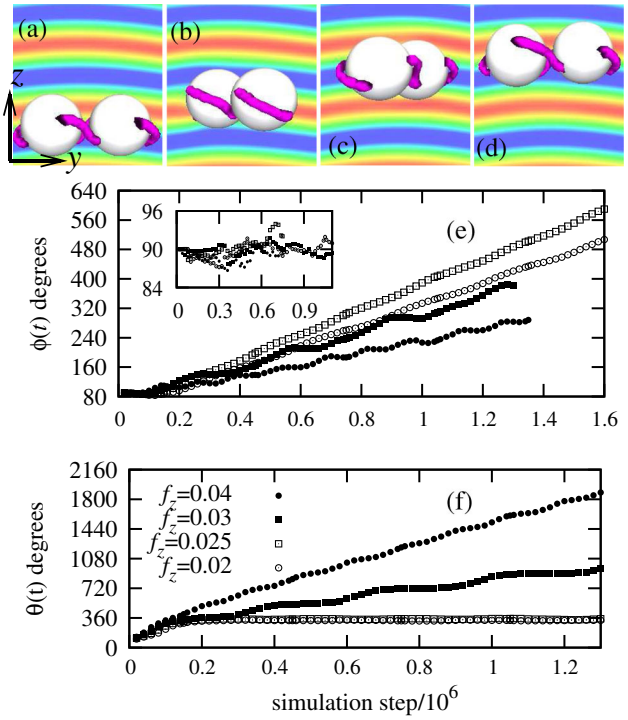


FIG. 2 (color online). (a)–(d) Snapshots of a steadily rotating dimer over a translation of half a pitch (a rotation of 180°). The director field is color coded according to the local director (red along $x$, blue along $y$). The time evolution of (e) $\phi$ and (f) $\theta$ [defined in Fig. 1(c)], for the rotor (open symbols) and phase slippage (closed symbols) motion. The inset in (e) also shows the angle between **d** and the helical axis, which remains close to 90°.

(closed symbols), now increases with time in a series of steps. These steps correspond to intervals with and without significant rotation of the dimer as it moves along the helix (see [11] for a movie and further discussion of the dynamics). Correspondingly, the phase lag $\theta(t)$ fails to reach a steady value [Fig. 2(f), closed symbols], but increases indefinitely. We refer to this as "phase slippage." There is a clear transition between the smooth "rotor" regime and the phase slippage regime.

Figure 3(a) quantifies the dependence of the average rotational velocity of the dimer $\Omega$ on the applied force for simulations at a range of force values. It can be seen that $\Omega$ is proportional to $f$ in the low-force rotor regime, while it decreases in the high-force phase slippage regime. Figure 3(b) shows the dependence of the average speed of the dimer along the helical axis with force, again showing a transition. However, it is difficult to relate these transitions to the equilibrium potential which is strictly valid only at Er $= 0$. Although the largest Eriksen number remains low (Er $\approx 0.026$), the potential is likely to be affected by dynamical effects including the local bending of the cholesteric layers [visible in Figs. 2(a)–2(d) [11]). The local bending of the layers for Er $\ll 1$, was also observed for a single colloid moving along the helical axis [5].

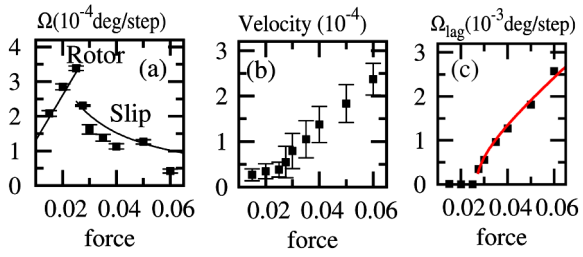


FIG. 3 (color online). Average rotational velocity ($\Omega$) (a) and sedimentation velocity (b) of the colloidal dimer as a function of the forcing. The nonlinear fit in (a) is $\Omega = c/f$, with $c > 0$ a constant. (c) shows $\Omega_{\rm lag}$ as a function of $f$ together with a fit to $d\sqrt{f^2 - f_c^2}$, with $d > 0$ a constant and $f_c \approx 0.0267 \pm 0.0005$.

To understand the dynamical transition better, we write down a set of phenomenological equations for the evolution of the dimer position, $z(t)$, and for $\phi(t)$, which gives the direction of **d** in the lab frame [Fig. 1(c)]. We assume that the basic features of the cholesteric ordering may be captured by an effective angular potential, also periodic in $z$: $V(\phi, z)$. Our equations read as follows,

$$\frac{d\phi}{dt} = -\frac{1}{\gamma_\phi}\frac{\partial V(\phi,z)}{\partial \phi}, \qquad \frac{dz}{dt} = -\frac{1}{\gamma_z}\frac{\partial V(\phi,z)}{\partial z}, \tag{3}$$
$$V(\phi,z) = -A\cos[B(\phi - q_0 z)] + fz.$$

Here, $A$ (units of energy) and $B$ (dimensionless) are positive constants, $f$ is the external forcing, while $\gamma_\phi$ and $\gamma_z$ are relaxational constants related to the rotational and translational friction of the dimer, and whose exact values we will not need. Equations (3) may be solved by an ansatz suggested by the behavior in Fig. 2(f). We write $\phi(t) = \Omega t + \theta(f)$, where the director-dimer angle follows the most favorable orientation apart from a phase lag, $\theta(f)$. This ansatz is a solution provided that $f$ is smaller than a critical threshold $f_c$, i.e., in the rotor phase. By estimating the average terminal velocity of the dimer as $f/\gamma_\phi$, we find that in the rotor phase the angular velocity is $\Omega \sim 2\pi f/(\gamma_z p)$ (this is true within statistical error using data in Fig. 3), and that the critical force is $f_c = A\gamma_z p/(2\pi\gamma_\phi)$. Above this threshold, $\theta$ increases with time as in Fig. 2(f) (solid symbols). The asymptotic velocity $\Omega_{\rm lag}[= d\theta(t)/dt] \sim \sqrt{f^2 - f_c^2}$ [11] for $f \to f_c$ provides a useful "order parameter" to characterize the rotor-slippage transition. In contrast, the angular velocity $\Omega$ decreases as $1/f$ for large $f$.

Importantly, Eqs. (3) capture both the near-critical behavior of $\Omega_{\rm lag}$, and the large $f$ behavior of $\Omega$ shown by our full LB simulations [see Fig. 3(a) for an $\Omega \sim 1/f$ fit and Fig. 3(c) for a $\Omega_{\rm lag} \sim \sqrt{f^2 - f_c^2}$ fit]. The near-critical behavior of $\Omega_{\rm lag}$ in our transition is similar to that of the velocity of a chain of driven particles in a periodic potential described by the Frenkel-Kontorova model [8], suggesting that our dimer provides a liquid crystal representative of a

wider class of models [11]. Another analogue is with the synchronization of two driven oscillators described by the Kuramoto model [9,11], where synchronized and unsynchronized states correspond to the rotor and slippage regimes, respectively. At the same time, we note that the physics of our cholesteric dimers is richer than that in Eqs. (3). Whereas the symmetry of the problem suggests that there should always be a very-low-force regime in which the dimer behaves as a rotor, the existence of the phase slippage regime at higher forces depends on the form of the effective pair potential. The required conditions hold for tangential anchoring but, according to our preliminary studies is violated in the normal anchoring case, for which we have not observed a phase-slip regime.

Our study may be viewed as a generalization of a classical problem: the sedimentation of two spheres in a viscous fluid. Intriguingly, Fig. 3(b) shows that the velocity-force curves are not linear, even in the Stokes limit of effectively zero Reynolds number. Rather, they appear to have different slopes (i.e., effective viscosities) in the rotor and phase slippage regimes. This is different to what occurs for a single sedimenting particle in a cholesteric, which leads to a linear velocity-force relation in the force range simulated here [5]. This biphasic force-velocity curve is due to the dynamic transition we discussed, and has no counterpart in classical sedimentation, in either Newtonian or Maxwell fluids. In the Newtonian case, sinking side by side speeds up the particles, by up to a factor of 2 [18], which is not true in our rotor phase (where we find that a dimer sediments slower than a single particle). In a Maxwell fluid, the repulsive or attractive interaction between two spheres sedimenting side by side is controlled by normal stresses [19]. In our case, we find a novel velocity-dependent torque and a dramatic dependence on the nature of the anchoring.

In conclusion, we have studied the equilibrium and dynamic properties of two colloidal spheres in a cholesteric liquid crystal. We have seen that chirality leads to a major change in the effective potential felt by the pair, with respect to the nematic limit. The elastic forces we find lead to the stabilization of a dimer at an angle of either 0° or 90°, as opposed to the 30° found in nematics. These results, alongside those of Ref. [6], suggest that it would be instructive to repeat the experiments performed in Ref. [7] with a cholesteric liquid crystal. Based on our results, one may also speculate that variations in particle size (or cholesteric pitch) can affect the local free energy landscape of colloidal suspensions in liquid crystals, and potentially drive the self-assembly of different structures.

Our main result is that, when subjected to an external force, the dimer rotates, either smoothly as a corkscrew or intermittently, with phase slippage. This transition occurs as the forcing exceeds a critical threshold: its value may be estimated via a simple theory considering the interplay between a spatially periodic angular potential and an external driving. The existence of the phase slippage regime is, however, highly nontrivial and relies on a delicate balance in the equilibrium and dynamic properties of our dimers: for example, we have not observed it for dimers with normal anchoring. An interesting possibility for future research would be to study the effects of external electric field applied to our colloidal dimer, as done with platelets [20] and nematic colloids [21], where unusual dynamics was triggered by the field.

This work was funded by EPSRC Grants No. EP/E030173 and No. EP/E045316. M. E. C. is funded by the Royal Society.

[1] C. E. Singa *et al.*, Proc. Natl. Acad. Sci. U.S.A. **107**, 535 (2009); P. Tierno *et al.*, Phys. Rev. Lett. **101**, 218304 (2008).
[2] M. Ravnik *et al.*, Phys. Rev. Lett. **99**, 247801 (2007); J. C. Loudet *et al.*, Langmuir **20**, 11336 (2004).
[3] T. Araki and H. Tanaka, Phys. Rev. Lett. **97**, 127801 (2006).
[4] M. Skarabot *et al.*, Phys. Rev. E **77**, 061706 (2008); M. Conradi *et al.*, Soft Matter **5**, 3905 (2009).
[5] J. S. Lintuvuori *et al.*, Phys. Rev. Lett. **105**, 178302 (2010); J. Mater. Chem. **20**, 10547 (2010).
[6] F. E. Mackay and C. Denniston, Europhys. Lett. **94**, 66003 (2011).
[7] I. I. Smalyukh *et al.*, Phys. Rev. Lett. **95**, 157801 (2005).
[8] J. Frenkel and T. Kontorova, Zh. Eksp. Teor. Fiz. **8**, 1340 (1938); R. Besseling, R. Niggebrugge, and P. H. Kes, Phys. Rev. Lett. **82**, 3144 (1999); R. Besseling *et al.*, Europhys. Lett. **62**, 419 (2003).
[9] J. A. Acebron *et al.*, Rev. Mod. Phys. **77**, 137 (2005).
[10] A. N. Beris and B. J. Edwards, *Thermodynamics of Flowing Systems* (Oxford University Press, Oxford, 1994).
[11] See Supplemental Material at http://link.aps.org/supplemental/10.1103/PhysRevLett.107.267802 for additional details on our model and dynamical transition and for movies of the dynamics.
[12] J.-B. Fournier and P. Galatola, Europhys. Lett. **72**, 403 (2005).
[13] D. Marenduzzo *et al.*, Phys. Rev. E **76**, 031921 (2007); M. E. Cates *et al.*, Soft Matter **5**, 3791 (2009).
[14] N.-Q. Nguyen and A. J. C. Ladd, Phys. Rev. E **66**, 046708 (2002).
[15] M. R. Mozaffari *et al.*, Soft Matter **7**, 1107 (2011).
[16] U. Tkalec *et al.*, Phys. Rev. Lett. **103**, 127801 (2009).
[17] $\theta \approx 348°$ and $\theta \approx 330°$, for $f = 0.25$ and $f = 0.2$, respectively. These correspond to $\theta = 12°$ and $\theta = 30°$ in the inset of Fig. 1(a).
[18] M. Stimpson and G. B. Jeffery, Proc. R. Soc. A **111**, 110 (1926).
[19] A. S. Khair and T. M. Squires, Phys. Rev. Lett. **105**, 156001 (2010).
[20] C. P. Lapointe *et al.*, Phys. Rev. Lett. **105**, 178301 (2010).
[21] O. P. Pishnyak *et al.*, Phys. Rev. Lett. **106**, 047801 (2011); O. P. Lavrentovich *et al.*, Nature (London) **467**, 947 (2010).